Titration of Ce^{3+} Ions in the $CeO_2(111)$ Surface by Au Adatoms

Yi Pan,[1] Niklas Nilius,[1,2,*] Hans-Joachim Freund,[1] Joachim Paier,[3,†] Christopher Penschke,[3] and Joachim Sauer[3]

[1]*Fritz-Haber-Institut der MPG, Faradayweg 4-6, 14195 Berlin, Germany*

[2]*Carl von Ossietzky Universität Oldenburg, Institut für Physik, D-26111 Oldenburg, Germany*

[3]*Humboldt-Universität zu Berlin, Unter den Linden 6, 10099 Berlin, Germany*

(Received 23 August 2013; revised manuscript received 19 September 2013; published 12 November 2013)

The role of surface and subsurface O vacancies for gold adsorption on crystalline $CeO_2(111)$ films has been investigated by scanning tunneling microscopy and density functional theory. Whereas surface vacancies serve as deep traps for the Au atoms, subsurface defects promote the formation of characteristic Au pairs with a mean atom distance of two ceria lattice constants (7.6 Å). Hybrid density functional theory calculations reveal that the pair formation arises from a titration of the two Ce^{3+} ions generated by a single O vacancy. The Au-Ce^{3+} bond forms due to a strain effect, as the associated charge transfer from the spacious Ce^{3+} into the adgold enables a substantial relaxation of the ceria lattice. Also the experimentally determined Au-pair length is reproduced in the calculations, as we find a Ce^{3+}-Ce^{3+} spacing of two ceria lattice parameters to be energetically preferred. Single Au atoms can thus be taken as position markers for Ce^{3+} ion pairs in the surface, providing unique information on electron-localization phenomena in reduced ceria.

DOI: 10.1103/PhysRevLett.111.206101 PACS numbers: 68.37.Ef, 71.15.Mb, 73.20.Hb, 73.61.Ng

Ceria in combination with precious metals (Pt, Au) features outstanding properties in a variety of catalytic processes, such as the water-gas-shift reaction and the low-temperature CO oxidation [1–3]. The high catalytic activity was interpreted as a cooperative effect of charge donation from the metal, resulting in Ce^{3+} formation, and oxygen spillover from the ceria lattice [4]. Although circumstantial evidence could be provided in support of this scenario, an atomistic verification of the mechanism, especially of the metal-oxide charge transfer, could not be given so far. In fact, even fundamental questions, such as the charge state of individual metal atoms on ideal and defective $CeO_2(111)$ surfaces lack definite answers.

From a theoretical point of view, there is agreement in the nature of Au binding to surface O defects, as being mediated by a charge transfer from adjacent Ce^{3+} ions into the adatom [5,6]. In contrast, formation of both neutral and positively charged gold is proposed on ideal surfaces, and no consensus has been reached on the preferred Au binding site that is either a surface O^{2-} or an O-O bridge site [5–7]. Moreover, possible Ce^{3+} adsorption sites have not been considered by theory so far.

The experimental situation for the Au/ceria system is even less satisfactory. In nonlocal X-ray spectroscopy studies, formation of Ce^{3+} species has been observed upon Au dosing onto $CeO_2(111)$; however, the charge state of the gold was not determined [8]. Other studies reported the formation of positively charged gold, but could not connect this data to the presence of specific defects in the surface [9,10]. The main reason for this uncertainty is the lack of atomic-scale information that is however of pivotal importance to accurately describe the Au-ceria redox properties. Direct correlation between a predominant Au adsorption scheme and the defect topology requires a local view onto the surface, as provided by scanning tunneling microscopy (STM). Examples for a successful elucidation of charge-transfer processes on ideal and defective oxides are the Au adsorption studies on alumina, magnesia, and vanadia films [11,12]. For ceria, the experiments mainly focused on defects in the uncovered surface so far [13–15].

In this Letter, we analyze the interaction of Au atoms with O vacancies in the $CeO_2(111)$ surface. From the abundance of atom pairs observed upon low-temperature gold deposition, we conclude that Au is able to decorate the Ce^{3+} ions generated by oxygen removal from the lattice. Our density-functional theory (DFT) calculations attribute this unusual binding behavior to a reduction of lattice strain induced by spacious Ce^{3+} ions in the oxide surface [16]. By transferring the extra charges into the Au atoms, the surface tension is reduced, which in turn reinforces the Au-Ce bond.

The experiments were performed with an ultrahigh-vacuum STM operated at liquid helium temperature. Ceria films of 5–8 trilayer thickness were prepared by cerium deposition onto a sputtered and annealed Ru(0001) single crystal in 5×10^{-7} mbar O_2 at room temperature. To promote long-range ordering, the oxide was annealed to 1000 K until a sharp hexagonal spot pattern became visible in low-energy electron diffraction, indicative for the presence of wide $CeO_2(111)$ patches. The quality of our films was confirmed by STM images that showed atomically flat terraces with triangular or hexagonal shapes and diameters as large as 50 nm [Fig. 1(a)]. The oxide defect structure was found to depend on the final annealing step. While annealing in O_2 triggered the formation of subsurface vacancies (V_{sub}), appearing as

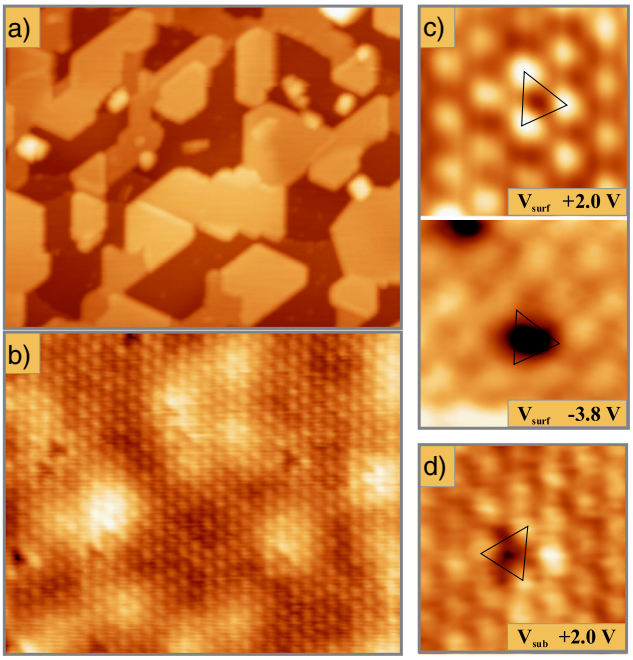

FIG. 1 (color online). (a) Overview (120×100 nm^2) and (b) atomically resolved STM image (10.5×8.5 nm^2) of a five trilayer thick $CeO_2(111)$ film grown on Ru(0001) ($U_s = +2.0$ V). The defects in (b) are mainly subsurface O vacancies. (c),(d) High resolution images of surface (V_{surf}) and subsurface O vacancies (V_{sub}) measured at positive and negative sample bias (2×2 nm^2). All STM data have been obtained at 25 pA current.

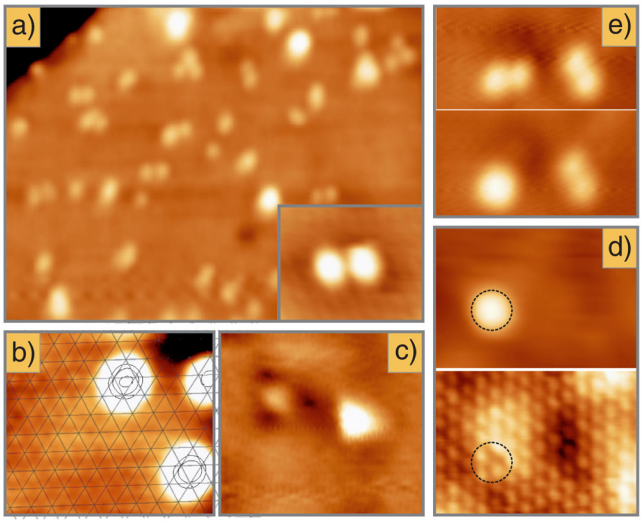

FIG. 2 (color online). (a) Ceria surface after dosing 0.05 ML of Au at 10 K (2.5 V, 26×20 nm^2). Note the abundance of atom pairs on the surface. The pair in the inset shows a pronounced sombrero shape, indicating its charged nature. (b) STM image showing the Ce sub-lattice and three Au atoms bound to regular O-top sites. (c) Au atoms sitting in a V_{surf} defect (left) and a regular lattice site (right) (both 3.8×3.0 nm^2). (d) Au adatom bound to a subsurface defect, as deduced from the atomically resolved image taken after atom removal with the tip (both 4.2×3.0 nm^2). (e) Transformation of an Au atom pair into an upright standing dimer via a tip-voltage pulse (5.5×3.0 nm^2).

trifoliate depressions in empty-state (positive bias) images, vacuum annealing mainly produced surface defects (V_{surf}) [13,14]. The V_{surf} showed up as holes and twofold or threefold maxima in filled and empty-state images, respectively [Fig. 1(c)]. The specific positive-bias contrast relates to the spill-out of $4f$ orbitals of adjacent Ce^{4+} ions, while Ce^{3+} species next to the vacancy appear slightly darker in the STM images [15]. The defect density was determined to be $\sim 5 \times 10^{12}$ cm^{-2} for V_{sub} at O_2-rich preparation conditions, and $\sim 5 \times 10^{13}$ cm^{-2} for V_{surf} defects formed upon 1000 K vacuum annealing [Fig. 1(b)].

Small quantities of gold were dosed from a tungsten filament directly onto the cryogenic sample at 10 K. The arriving atoms had only limited transient mobility and mainly remained isolated on the surface [Fig. 2(a)]. At positive sample bias, Au monomers were imaged as simple protrusions with 1.5 Å height and 10 Å diameter, while Au aggregates featured larger heights of 3–5 Å [17]. The role of lattice defects in the adsorption behavior was derived from a closer inspection of appearance and binding position of the Au atoms. The STM image in Fig. 2(b), taken on an ideal oxide region, shows the atomically resolved Ce sublattice with three Au atoms bound atop. The position of the surface and subsurface O sites in the lattice was determined by evaluating the orientation of nearby equilibrium step edges, as displayed in Fig. 1. Based on geometrical considerations discussed in Ref. [18], the downward pointing triangles in Fig. 2(b) correspond to O-top positions, while the upright triangles mark the subsurface O^{2-} ions. This assignment was cross-checked against the position of surface and subsurface O defects that were indeed found at the expected lattice sites. With this input, the O-top position was identified as preferred Au adsorption site on the ideal $CeO_2(111)$ surface, although O-O bridge sites have been detected as well.

Further binding geometries emerged in the presence of lattice defects. As expected, surface vacancies turned out to be effective traps for the Au atoms, from which they could not be removed with the STM tip anymore [Fig. 2(c)] [5,6]. Such defect-bound species served as nucleation centers for incoming Au atoms and governed the aggregation processes on the surface [17]. However, also subsurface defects, more precisely the Ce^{3+} ions associated with them, were found to modify the adsorption behavior. Experimental evidence came from the unusual arrangement of Au atoms on oxide films with a high density of V_{sub} defects. At low exposure, up to 40% of the Au species appeared as characteristic pairs with a mean atom distance of 7.6 Å (two CeO_2 lattice parameters) [Fig. 2(a)]. Note that even the shortest pair length of 4.8 Å observed here would be too large to enable direct Au-Au coupling [Fig. 3(a)]. We therefore suggest that this unusual atom

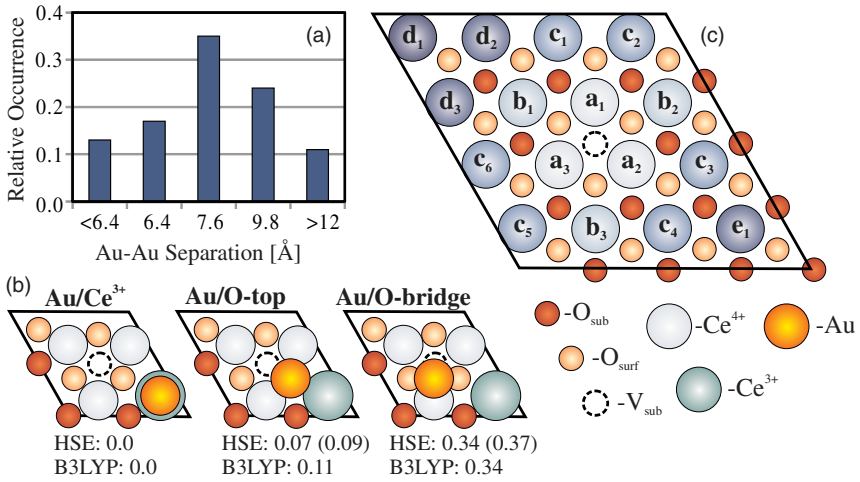

FIG. 3 (color online). (a) Distance histogram determined for ~150 Au pairs on the ceria surface. (b) Relative energies [eV] obtained using HSE (optimized) and B3LYP (single point) for three relevant Au adsorption sites (Values in parenthesis include dispersion effects). (c) $p(4 \times 4)$ unit cell with the notation of different Ce coordination shells around the V_{sub} defect, as used in Table I.

distribution is governed by defects in the ceria lattice. The atom pairs were found to be metastable, as they could be assembled to a single upright Au_2 dimer with a 3.0 V tip pulse [Fig. 2(e)]. Further manipulation experiments enabled us to determine the binding sites of the paired atoms by desorbing them via high bias scanning. In a few successful examples, we could identify a subsurface vacancy in close vicinity to the Au pair, suggesting an involvement of this defect type in the pair formation [Fig. 2(d)]. This idea is supported by a statistical analysis of our data that revealed a direct dependence of the number of Au pairs on the V_{sub} concentration in the surface [19]. Finally, all atoms in paired configurations but also a couple of isolated monomers featured a specific contrast in low bias images, characterized by a dark ring around the actual maximum [Fig. 2(a), inset]. In earlier experiments on alumina [11] and magnesia films [20], such sombrero shapes were associated with charges on the adatoms, inducing a local bending of the surrounding oxide bands. We thus conclude that V_{sub} defects are not only responsible for the pair formation, but induce a charge transfer into the Au atoms as well. As a working hypothesis, we propose that the Au pairs result from a titration of the Ce^{3+} surface species created by oxygen removal from the ceria lattice.

To corroborate this scenario, we have performed spin-polarized DFT calculations as implemented in VASP [21]. The electron-ion interaction was described with the projector augmented wave method, including scalar relativistic corrections and a kinetic energy cutoff of 600 eV [22]. To simulate isolated V_{sub} defects at high and low concentrations, we used a $p(2 \times 2)$ and a $p(4 \times 4)$ unit cell comprising three O-Ce-O trilayers, respectively. The Brillouin zone was sampled on a 2×2 k-point grid and the Γ point for the two models. To overcome shortcomings of conventional GGA + U, all calculations were performed with the screened hybrid functional HSE [23,24]. Dispersion effects were included by using a pairwise summed C_6/R^6 term [25], parameterized with values for Au and Ce from the literature [26,27]. To demonstrate the robustness of our conclusions, we reproduced selected data points using the B3LYP hybrid functional.

In a first approach, we have explored the adsorption energies of Au atoms in the presence of subsurface O defects in a $p(2 \times 2)$ configuration [19]. Depending on the functional, the Ce^{3+} position was found to be preferred by 70–110 meV with respect to the O-top site, while O-O bridge positions were pronouncedly less stable [Fig. 3(b)]. The adsorption energies for Au slightly varied with the alignment of the two Ce^{3+} spins, with a ferromagnetic coupling [Fig. 3(b)] being 30 meV lower in energy than an antiferromagnetic one. In the preferred binding position, the $4f$ electron of Ce^{3+} gets transferred into the Au $6s$ orbital, generating a Ce^{4+} and an Au^-. The charge transfer is possible, because the Au $6s$ orbital is energetically close to the occupied $4f$ orbital of Ce^{3+} (Fig. 4). Already these findings are able to explain the effect of Ce^{3+} titration and the sombrero shape that can

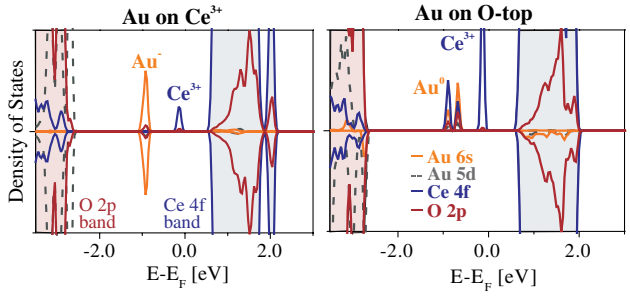

FIG. 4 (color online). Projected local density of states (with HSE) for an Au atom bound to a Ce^{3+} and an O^{2-}-top site in a $p(2 \times 2)$ cell.

be taken as experimental fingerprint for charged Au species on the ceria surface.

In a next step, we have analyzed the origin of the Au-Ce^{3+} binding preference, in particular the role of lattice strain in reduced $CeO_2(111)$. For this purpose, we used the larger $p(4 \times 4)$ cell to simulate the V_{sub} defect. In the dilute limit, the energetic ordering for Au adsorption reversed and binding to O-top sites became favorable by 70 meV with respect to the Ce^{3+} sites. Moreover, only a partial electron transfer occurred when fixing the Au on top of Ce^{3+} and the resulting electron configuration was closer to $Ce^{3+}(4f^1)/Au^0(6s^1)$. This difference reflects the impact of surface tension in reduced ceria on the Au adsorption behavior. Given the large ion radius of Ce^{3+} compared to Ce^{4+} (1.01 versus 0.87 Å), a substantial lattice strain builds up when reducing the oxide film [16]. Electron transfer from surface Ce^{3+} to the Au atoms now provides an effective means to release this strain, which in turn stabilizes the Au-Ce bond. The effect of Ce^{3+} titration is therefore expected to occur only in regions with a high number of reduced Ce species. Although we cannot pinpoint the critical Ce^{3+} density at which the Au adsorption swaps from Ce^{3+} to O-top sites, we want to emphasize that large variations were observed in the abundance of Au-atom pairs, suggesting a decisive influence of the local oxide reduction state.

To further support the Ce^{3+} titration scenario, we compared the experimentally determined Au-Au pair distances [Fig. 3(a)] with the equilibrium separation of the two Ce^{3+} created by a single O subsurface defect. For this purpose, the Ce^{3+}-V_{sub} configuration as well as the Ce^{3+} pair distance were varied systematically within the $p(4 \times 4)$ cell [19]. In extension to earlier data [15,16,28], we found not only a preference for electron localization away from the V_{sub} defect, but determined the optimum arrangement of the associated Ce^{3+} ions (Table I). The lowest defect formation energy, as calculated with respect to $\frac{1}{2}O_2$, was revealed when both Ce^{3+} sit in the 2nd coordination shell of the defect and are 7.6 Å apart [Fig. 3(c), (b_1–b_3) configuration]. This value agrees well with the maximum in the Au pair length derived from experiment. When moving one Ce^{3+} into the 1st coordination shell, the formation energy rises by 160 meV if both Ce^{3+} ions are opposite to each other (a_1-b_3) and by 230 meV if they locate on neighboring sites (a_3-b_3). All other configurations have even higher formation energies, in particular when the Ce^{3+} pair occupies nearest neighbor sites to the V_{sub} (a_1-a_3). Apparently, the Ce^{3+} repel each other and prefer configurations, in which both ions sit in the 2nd coordination shell of the defect and are spaced by two lattice constants.

In summary, we have demonstrated that Au adatoms are able to titrate Ce^{3+} ions in a reduced $CeO_2(111)$ surface. The associated charge transfer into the gold is promoted by the release of lattice strain, as spacious Ce^{3+} transform into small Ce^{4+} species. The Au decoration effect can be exploited to determine the position of Ce^{3+} ions at the atomic scale, addressing the essential question of electron localization in defective ceria.

TABLE I. Structure and vacancy formation energy (E_{def}) with respect to $\frac{1}{2}O_2$ for different subsurface O vacancy/Ce^{3+} configurations obtained with HSE.

Ce^{3+} configuration	Ce^{3+}-Ce^{3+} distance [Å]	Ce^{3+}-defect distances [Å]	$E_{def}(\frac{1}{2}O_2)$ [eV]	
			High spin	Low spin
b_1–b_3	7.67	4.41; 4.42	**2.26**	2.34
a_1–b_3	6.77	2.33; 4.44	2.42	2.41
b_3–c_6	6.65	4.41; 5.84	2.48	
a_3–b_3	3.87	2.34; 4.42	2.49	2.55
b_3–d_3	10.11	4.40; 7.94	2.51	
c_5–c_6	3.88	5.84; 5.85	2.60	
c_1–c_6	7.65	5.85; 5.84	2.61	
a_1–d_3	7.63	2.35; 7.93	2.62	
a_3–c_5	3.77	2.32; 5.86	2.63	
a_1–a_3	4.09	2.37; 2.37	2.71	2.70

The DFG excellence cluster 'UNICAT', the COST action CM1104, the HLRN cluster of the North-German Supercomputing Alliance, and the JUROPA cluster (Jülich) are acknowledged for support.

Note added in proof.—We recently found another structure for Au bound atop Ce^{3+}, where charge-transfer occurs from Ce^{3+} in a subsurface position to the ad-gold. The energy of this structure is even lower by 120 meV than the one shown in Fig. 3(b).

*Corresponding author.
nilius@fhi.mpg-berlin.de
†Corresponding author.
joachim.paier@chemie.hu-berlin.de

[1] A. Trovarelli, *Catalysis by Ceria and Related Materials* (Imperial College Press, London, 2002).
[2] Q. Fu, H. Saltsburg, and M. Flytzani-Stephanopoulos, Science **301**, 935 (2003).
[3] J. Rodriguez, Catal. Today **160**, 3 (2011).
[4] G. N. Vayssilov *et al.*, Nat. Mater. **10**, 310 (2011).
[5] C. J. Zhang, A. Michaelides, and S. J. Jenkins, Phys. Chem. Chem. Phys. **13**, 22 (2011).
[6] J. Paier, C. Penschke, and J. Sauer, Chem. Rev. **113**, 3949 (2013).
[7] M. Nolan, S. C. Parker, and G. W. Watson, Surf. Sci. **595**, 223 (2005); C. Loschen, A. Migani, S. T. Bromley, F. Illas, and K. M. Neyman, Phys. Chem. Chem. Phys. **10**, 5730 (2008); M. M. Branda, N. J. Castellani, R. Grau-Crespo, N. H. de Leeuw, N. C. Hernandez, J. F. Sanz, K. M. Neyman, and F. Illas, J. Chem. Phys. **131**, 094702 (2009).
[8] M. Škoda, M. Cabala, I. Matolínová, K. C. Prince, T. Skála, F. Šutara, K. Veltruská, and V. Matolín. J. Chem. Phys. **130**, 034703 (2009).

[9] Q. Fu, W. Deng, H. Saltsburg, and M. Flytzani-Stephanopoulos, Appl. Catal., B **56**, 57 (2005); R. Si, J. Tao, J. Evans, J. B. Park, L. Barrio, J. C. Hanson, Y. Zhu, J. Hrbek, and J. A. Rodriguez. J. Phys. Chem. C **116**, 23 547 (2012).

[10] M. Baron, O. Bondarchuk, D. Stacchiola, S. Shaikhutdinov, and H.-J. Freund, J. Phys. Chem. C **113**, 6042 (2009); K. Naya, R. Ishikawa, and K. Fukui, J. Phys. Chem. C **113**, 10 726 (2009).

[11] N. Nilius, M. V. Ganduglia-Pirovano, V. Brázdová, M. Kulawik, J. Sauer, and H.-J. Freund, Phys. Rev. Lett. **100**, 096802 (2008).

[12] N. Nilius, V. Brázdová, M.-V. Ganduglia-Pirovano, V. Simic-Milosevic, J. Sauer, and H.-F. Freund, New J. Phys. **11**, 093007 (2009).

[13] F. Esch, S. Fabris, L. Zhou, T. Montini, C. Africh, P. Fornasiero, G. Comelli, and R. Rosei, Science **309**, 752 (2005).

[14] S. Torbrügge, M. Reichling, A. Ishiyama, S. Morita, and Ó. Custance, Phys. Rev. Lett. **99**, 056101 (2007).

[15] J.-F. Jerratsch, X. Shao, N. Nilius, H.-J. Freund, C. Popa, M. V. Ganduglia-Pirovano, A. M. Burow, and J. Sauer, Phys. Rev. Lett. **106**, 246801 (2011).

[16] M. V. Ganduglia-Pirovano, J. L. F. Da Silva, and J. Sauer, Phys. Rev. Lett. **102**, 026101 (2009).

[17] Y. Pan, Y. Cui, N. Nilius, and H.-J. Freund, J. Phys. Chem. C **117**, 21879 (2013).

[18] N. Nilius, S. M. Kozlov, J.-F. Jerratsch, M. Baron, X. Shao, S. Shaikhutdinov, H.-J. Freund, F. Viñes, and K. M. Neyman, ACS Nano **6**, 1126 (2012).

[19] See Supplemental Material at http://link.aps.org/supplemental/10.1103/PhysRevLett.111.206101 for statistical analysis of defect versus Au-pair numbers, computational details, and atomic coordinates used in the calculations.

[20] M. Sterrer, T. Risse, U. Martinez Pozzoni, L. Giordano, M. Heyde, H.-P. Rust, G. Pacchioni, and H.-J. Freund, Phys. Rev. Lett. **98**, 096107 (2007).

[21] G. Kresse and J. Furthmüller, Comput. Mater. Sci. **6**, 15 (1996).

[22] P. E. Blöchl, Phys. Rev. B **50**, 17 953 (1994); G. Kresse and D. Joubert, Phys. Rev. B **59**, 1758 (1999).

[23] J. Heyd, G. E. Scuseria, and M. Ernzerhof, J. Chem. Phys. **118**, 8207 (2003).

[24] A. V. Krukau, O. A. Vydrov, A. F. Izmaylov, and G. E. Scuseria, J. Chem. Phys. **125**, 224106 (2006).

[25] S. Grimme, J. Comput. Chem. **27**, 1787 (2006).

[26] K. Tonigold and A. Gross, J. Chem. Phys. **132**, 224701 (2010).

[27] C. Penschke, J. Paier, and J. Sauer, J. Phys. Chem. C **117**, 5274 (2013).

[28] H. Y. Li, H. F. Wang, X. Q. Gong, Y. L. Guo, Y. Guo, G. Lu, and P. Hu, Phys. Rev. B **79**, 193401 (2009).